Predissociation of Rydberg states of CO investigated by the detection of atomic fragments

doi: 10.1063/1.1363672

Predissociation of Rydberg states of CO investigated by the detection of atomic fragments

Akihiro Okazaki, Takayuki Ebata,[a] and Naohiko Mikami
Department of Chemistry, Graduate School of Science, Tohoku University, Sendai 980-8578, Japan

(Received 15 December 2000; accepted 19 February 2001)

Predissociation of Rydberg states of CO has been investigated by the C (^3P and ^1D) and O(^3P) photofragment measurements in the region of 103 000–114 000 cm^{-1} (88–97 nm). The simulations of the rotational structures of np and nf Rydberg states were also carried out by using the l-uncoupling Hamiltonian model. The photofragment yield spectra were compared with the ion-dip spectra which correspond to the absorption spectra, indicating that all the Rydberg states, ns, np, nd, and nf converging to the $X\,^2\Sigma^+$ CO^+ ion, were subject to the predissociation. It was found that the lower member $np\pi$ and $nd\pi$ states exhibit two dissociation path ways, that is the C(^3P) + O(^3P) and the C(^1D) + O(^3P) channels. Especially, for the $4p\pi L\,^1\Pi(v=0)$ state the two channels were found to be competitive with respect to parity as well as rotational quantum number J. At higher np series, such a parity and J-dependence of the predissociation disappeared, and the observed rotational structure was simulated very well by the model with no parity nor J dependence. For the $nd\sigma$ states, the spectra of the $3d\sigma$ and $5d\sigma(v=0)$ states were diffuse, while the $4d\sigma(v=0)$ state showed a rotationally resolved photofragment yield spectrum. All the photofragment yield spectra of the $nf(v=0)$ states exhibited sharp structures compared with those of other Rydberg states with a small l value. From a comparison between the photofragment yield spectrum and the ion-dip spectrum, it was found that the predissociation rate of the e-symmetry component is larger than that of the f-symmetry component. It was suggested that the e-symmetry levels predissociate through $D'\,^1\Sigma^+$ valence states, while the f-symmetry levels predissociate through the $2\,^1\Pi$ state. © *2001 American Institute of Physics.* [DOI: 10.1063/1.1363672]

I. INTRODUCTION

Carbon monoxide (CO) is the second most abundant molecule after H_2 in the interstellar medium. Because of an important role of the dissociation process of the medium in space, the absorption spectrum and the dissociation of the electronic excited states of CO have been extensively studied in the region of 90–115 nm. The absorption spectrum of the Rydberg series of CO was first measured by Ogawa and Ogawa.[1,2] They identified several Rydberg series converging not only to the ground state ($X\,^2\Sigma^+$) of CO^+ ion but also to its electronically excited states, and analyzed rotational structures for the Rydberg states up to $n=4$.

In an earlier stage of spectroscopic studies of CO, one-photon vacuum UV absorption spectroscopy was extensively performed for the rotational structure analysis and for the determination of absorption cross sections. Letzelter *et al.*[3] observed the absorption spectrum in the energy region of 88.5–115 nm, and reported the absorption cross section and the fluorescence quantum yield. They determined the photodissociation cross sections and concluded that the photodissociation of CO takes place after the transition to discrete states, most of which are thought to be Rydberg states. Eidelsberg and co-workers[4,5] have given a detailed analysis of the absorption spectrum of CO in the region 91–110 nm, providing the molecular constants of these states. In rather recent studies with laser spectroscopy, Ubachs and co-workers[6–9] and Drabbels *et al.*[10] reported the predissociation rates of the Rydberg states ($n=3-6$) by measuring the rotational linewidths with a narrow bandwidth laser. In these works, J-dependent predissociation has been found in some of the Rydberg states. The pulsed-field ionization (PFI) spectra from the single rotational level of the $3p\pi E\,^1\Pi(v=0)$ state were observed by Softley's group.[11] They investigated the Rydberg channel interactions occurring in very high Rydberg states. Rotationally resolved spectra of the Rydberg states ($n=4-7$ for $v=0$, $n=4-10$ for $v=1$) were observed by Ebata and co-workers[12–15] by using triple resonance spectroscopy. Because of its high selectivity on the rotational quantum number J as well as parity, the rotational structures of four Rydberg states (ns, np, nd, and nf) have been extensively analyzed.

When one pays attention to the dissociative states, two $^1\Sigma^+$ states correlating to the C(^3P) + O(^3P) dissociation channel are well characterized. One is the $X\,^1\Sigma^+$ ground state of CO, and the other is the $D'\,^1\Sigma^+$ state, which has been identified by Wolk and Rich[16] with laser-induced fluorescence spectroscopy. Especially, it has been thought that the $D'\,^1\Sigma^+$ valence state plays an important role for the predissociation of the Rydberg states. Especially, the ns Rydberg series is known to predissociate through the D' state, and Komatsu *et al.*[15] determined the potential curve of the repulsive D' state from the linewidth measurements of the $v=0$ and 1 levels of the ns states. According to the *ab initio* calculations by Cooper and Kirby,[17] the $3s\sigma\ B\,^1\Sigma^+$

[a]Author to whom correspondence should be addressed. Electronic mail: ebata@qclhp.chem.tohoku.ac.jp

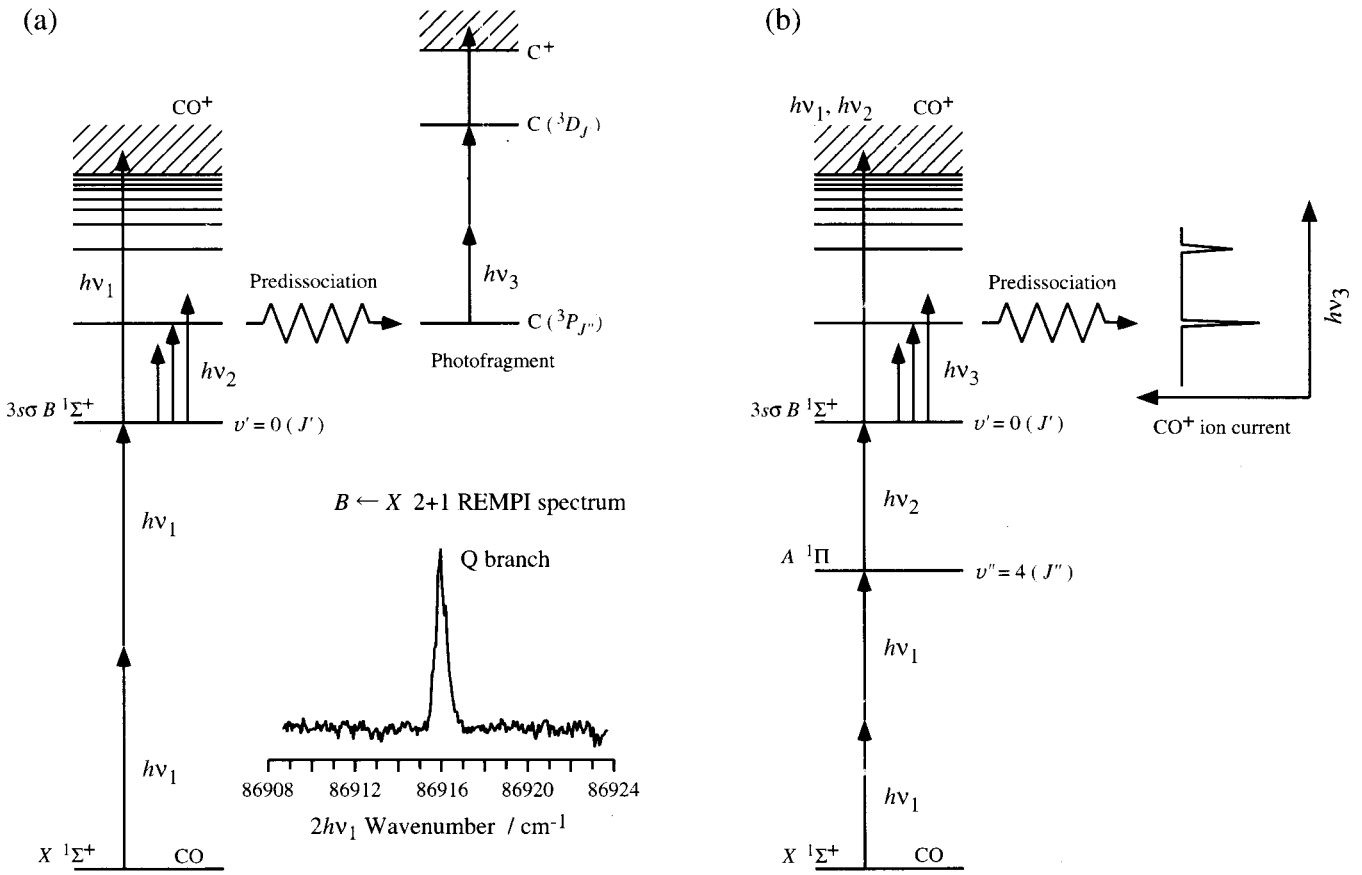

FIG. 1. Schematic excitation diagrams of (a) photofragment yield spectroscopy and (b) triple resonance ion-dip spectroscopy of CO.

and $D'\ ^1\Sigma^+$ states are strongly coupled with each other, resulting in a double minimum adiabatic potential surface. Tchang-Brillet *et al.*[18,19] obtained the potential curve of the $D'\ ^1\Sigma^+$ state in the region close to the $B\ ^1\Sigma^+$ state by using the close coupling method. Hiyama *et al.*[20,21] calculated the potential curves of the $D'\ ^1\Sigma^+$ and $2\ ^1\Pi$ valence states, and carried out the MQDT analysis of the superexcited states of CO. They analyzed the autoionization mechanism by comparing with the results of triple resonance spectroscopy done by Ebata *et al.*[13] Tennyson[22] has been carried out the *R*-matrix calculation of the Rydberg states up to $n=7$ of $v=0$ level and reported vertical excitation energies and quantum defects for these states.

Despite the extensive spectroscopic studies of the Rydberg states of CO, very few experiments have been done on the measurement of photofragment atoms produced by the predissociation process. Forch and Merrow[23,24] observed atomic oxygen generated after two-photon absorption of CO at 193 nm. Hill *et al.*[25] detected an emission of atomic carbons produced by the multiphoton dissociation of CO. However, none of those studies has specified the states from which the predissociation takes place. It is fundamentally important to specify the initial state for understanding the state-to-state dynamics of the predissociation, and for obtaining the potential curves of the repulsive valence states. In a previous paper, we examined the photofragment yield spectra of the $3d\pi L'\ ^1\Pi(v=1)$ and $4p\pi L\ ^1\Pi(v=0)$ states by monitoring the fragment atoms produced by the predissociation.[26] Two dissociation channels were identified for the two states. One is the channel leading to $C(^3P)+O(^3P)$ and the other is the channel leading to $C(^1D)+O(^3P)$, in which the latter channel is spin-forbidden. Predissociation rate constants for the two dissociation channels were obtained and it was found that the two channels compete with almost equal rate constants.

In the present work, we report our extended study on the predissociation of the $v=0$ level of the Rydberg states by measuring the atomic photofragment yield spectra. We observed the photofragment yield spectra in the region of 103 000–114 000 cm^{-1} (88–97 nm) and identified the Rydberg series converging to the $X\ ^2\Sigma^+$ state of the CO^+ ion. The observed photofragment yield spectra were then compared with the ion-dip spectra in the same energy region. In addition, the rotational structure of the Rydberg states was simulated by using the *l*-uncoupling Hamiltonian model. By comparing the observed spectra with the ion-dip and the simulated spectra, the predissociation mechanism of the np and nf series is discussed.

II. EXPERIMENT

The experimental setup and the excitation scheme have been already reported in a previous work.[26] Figure 1 shows the excitation schemes used in the present experiment, in which three different laser lights were used. For the photofragment measurement [Fig. 1(a)], the higher Rydberg state

of CO molecule was produced by the two-color (ν_1, ν_2) double resonance excitation through the $B\,^1\Sigma^+(v=0)$ state, and the generated C($^3P, ^1D$) or O(^3P) fragment was detected by two photon resonant three photon ionization, (2+1) REMPI. The $B \leftarrow X$ transition occurs by the two-photon absorption of ν_1. The inlet in Fig. 1(a) shows (2+1) REMPI spectrum of the $B \leftarrow X$ (0,0) transition. As seen in the spectrum, only an intense Q branch appears when linearly polarized light for ν_1 is used, so that several rotational levels are simultaneously pumped to the $B(v=0)$ state. The B state molecules were further excited to Rydberg states by ν_2. The fragment C or O atom generated by the predissociation of the Rydberg states was monitored by the (2+1) REMPI spectroscopy with a third laser (ν_3). For the C($^3P, ^1D$) detection, the $^3D_{J'} \leftarrow {}^3P_{J''}$ or $^1P_1 \leftarrow {}^1D_2$ transition was used, while the $^3P_{J'} \leftarrow {}^3P_{J''}$ transition was used for the O(^3P) detection. By scanning ν_2 while monitoring the carbon or oxygen ion signal, the photofragment yield spectra were obtained.

The experiment was performed under a jet-cooled condition of CO. Pure CO gas at the pressure of 3 atm was expanded into vacuum through a pulsed nozzle having a 400 μm orifice. The pressure of a vacuum chamber was 2×10^{-5} Torr during the operation. Two dye lasers (Lambda Physik FL3002 and Molectron DL14) were simultaneously pumped by a XeCl excimer laser (Lambda Physik LPX 100). The first laser (ν_1) was the frequency doubled output of FL3002, and its typical laser power was 30 μJ. The second laser (ν_2) was the fundamental output of one of the dye laser (DL14), and its typical laser power was 50 μJ. The laser beams of ν_1 and ν_2 were introduced into the vacuum chamber in a mutually counterpropagated geometry, and were focused by two lenses ($f=250$ mm). The bandwidths (FWHM) were 0.3 and 0.8 cm^{-1} for ν_1 and ν_2, respectively. A second harmonic output of the Nd:YAG laser pumped dye laser (Quanta-Ray GCR-230-10/Continuum ND6000) was used for ν_3, which was coaxially introduced with ν_2 by using a beam combiner. A typical ν_3 laser power was 400 μJ, with its FWHM of 0.3 cm^{-1}. All the laser beams were linearly polarized and crossed at 15 mm downstream from the free jet expansion. The delay time between ν_1 (or ν_2) and ν_3 was set to 10 ns by using a digital delay generator (SRS Model DG535). CO^+ and the fragment atomic ions were separated with a time-of-flight mass spectrometer, and detected by an electron multiplier (Murata Ceratron). The ion current was amplified by an amplifier (NF Model BX-31). An electric field ($\approx$70 V/cm) was applied to the interaction region in order to extract the ions into the flight tube. The signal were processed by a digital boxcar integrator (PAR Model 4420) connected with a personal computer. Frequencies of the lasers were calibrated by a calibrated 0.75 m double monochromator, and the accuracy of the laser frequencies was ± 1 cm^{-1}.

In order to compare with the photofragment yield spectra, the ion-dip spectra were also observed in the same energy region. The experimental setup for the ion-dip spectroscopy with the triple resonant excitation was described in previous papers,[14,15] and the experimental scheme is shown in Fig. 1(b). Briefly, jet-cooled CO was excited to a single rovibrational level ($v''=0$ and J'') of the $3s\sigma\,B\,^1\Sigma^+$ state by the double resonant excitation through the $A\,^1\Pi(v=4)$ state with two laser beams (ν_1, ν_2). A part of the CO molecules at the B state was further ionized by absorbing additional photons of ν_1 and/or ν_2. This ion signal was used as a measure of the CO population of the B state. Under this condition, the third laser (ν_3) was introduced to excite CO from the B state to the higher Rydberg states. Since most of the Rydberg states are predissociative, the CO molecules excited to the Rydberg states immediately dissociate, leading to a depletion of the B state population. Therefore, by scanning the ν_3 frequency while monitoring the ion signal, the ion-dip spectrum was obtained, representing the transition to the high Rydberg from the B state.

III. RESULTS AND DISCUSSION

As was described previously, in the experiment of the photofragment measurement, the high Rydberg states of CO were prepared by two-color double resonant excitation through the $3s\sigma\,B\,^1\Sigma^+(v=0)$ state. As shown in Fig. 1(a), the $B\,^1\Sigma^+ \leftarrow X\,^1\Sigma^+$ two-photon transition with a linearly polarized ν_1 exhibits an intense Q branch, so that the X state CO molecules populated in the rotational levels at given rotational temperature are simultaneously pumped to the B state by two ν_1 photons. Thus, the photofragment yield spectrum obtained by scanning ν_2 exhibits the transitions from those rotational levels of the $B(v=0)$ state.

In the Rydberg state having a high principle quantum number or a large electronic angular momentum l, the uncoupling of l with respect to the molecular axis occurs, and the coupling scheme changes from Hund's case (b) to (d). In Hund's case (d), each state is expressed by a linear combination of the case (b) basis set, such as Σ, Π, Δ, etc., and the rotational structures of the high Rydberg states of CO are calculated with the l-uncoupling Hamiltonian model. The rotational Hamiltonian of the singlet state is given as follows:

$$H_{\mathrm{rot}} = B[(N^2 - N_z^2) + (l^2 - l_z^2) - (N^+ l^- + N^- l^+)]. \qquad (1)$$

Here, $N(=J)$ and $N_z(=J_z)$ are the total angular momentum and its projection onto the molecular axis, respectively. l and l_z are the angular momentum of the Rydberg electron and its projection onto the molecular axis, respectively. The singlet np Rydberg state is composed of three Hund's case (b) basis sets, $^1\Sigma^+$, $^1\Pi^+$, and $^1\Pi^-$, so that this state is often called ''np complex.'' The rotational energy levels of the np complex are obtained by solving the energy matrix of the Hamiltonian given by Eq. (1), and the transition probability of the np Rydberg $\leftarrow B\,^1\Sigma^+$ is calculated from the obtained coefficients. The np Rydberg $\leftarrow B\,^1\Sigma^+$ transition consists of five branches, $^{-2}P_1$, $^0R_1$, $^0P_{-1}$, $^0Q_0$, and $^2R_{-1}$, which refer to the notation of $^{N^{+\prime}-N''}\Delta J_{\mathcal{L}'}$. Here, $N^{+\prime}$ is the angular momentum of the ion core, and $\mathcal{L}'$ is the projection of l onto the rotational axis of the high Rydberg state. N'' is the total angular momentum of the B state.

Since most of J levels in the X state populated in the jet were pumped to the B state via the Q branch excitation, we assumed the same rotational distribution for the $3s\sigma\,B\,^1\Sigma^+(v=0)$ state with that in the X state. The simulated photofragment yield spectra reproduced well the ob-

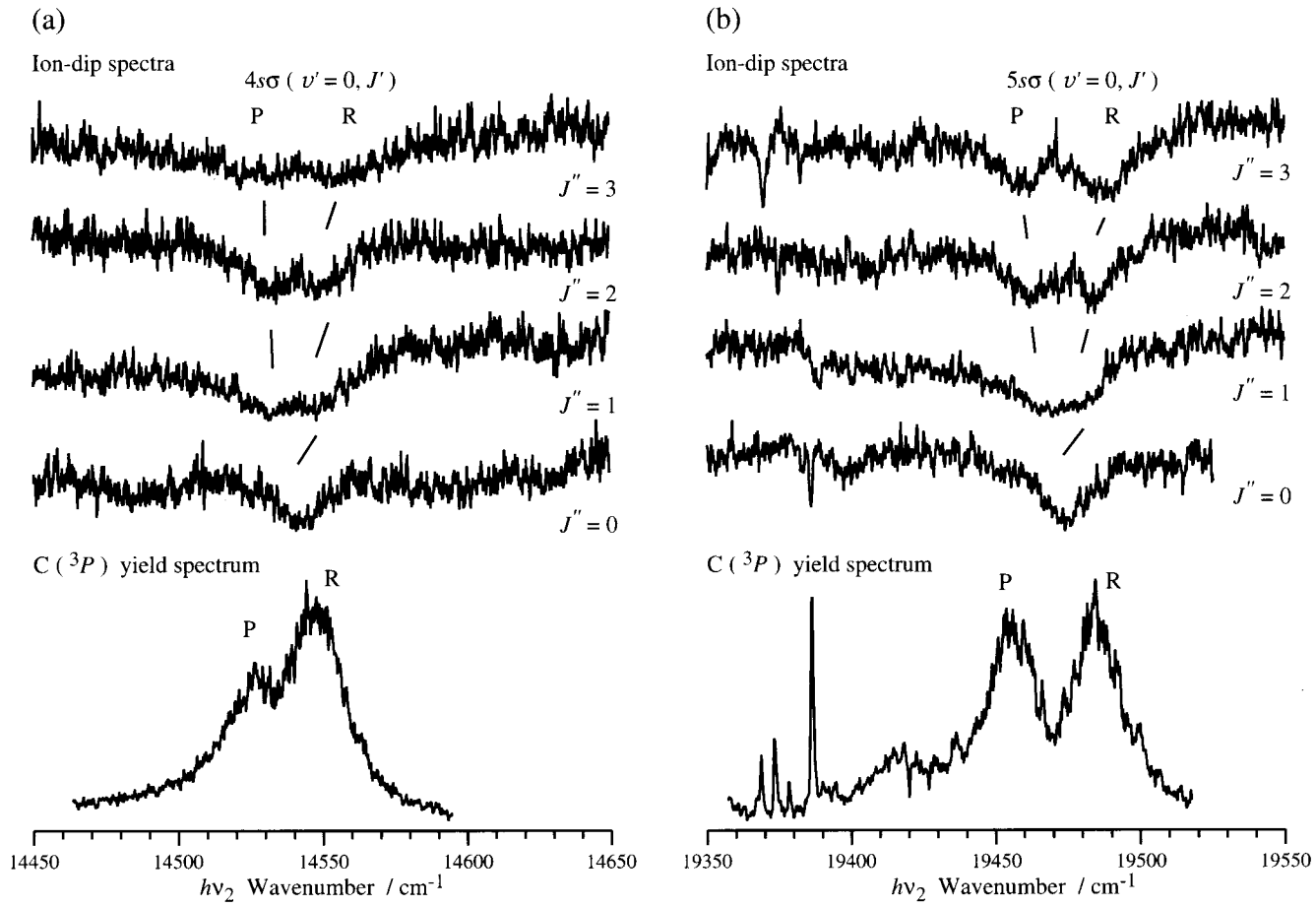

FIG. 2. $ns\sigma \leftarrow B\,^1\Sigma^+(v''=0)$ ion-dip spectra of CO (upper) and C(^3P) photofragment yield spectra (lower). (a) $4s\sigma(v'=0)$, (b) $5s\sigma(v'=0) \leftarrow B\,^1\Sigma^+(v=0)$ transition.

served photofragment yield spectra when we assumed $T_{\rm rot}=15$ K. The simulation of the rotational structure was also carried out for the nf Rydberg states. The nf Rydberg state ($l=3$) consists of seven $\mathcal{L}$ components, $\mathcal{L}=-3\mp3$, which are expressed also by the linear combination of the Hund's case (b) basis set. The even $\mathcal{L}$ component consisted of Π^-, Δ^-, and Φ^-, and the odd $\mathcal{L}$ component consisted of Σ^+, Π^+, Δ^+, and Φ^+. The $nf \leftarrow B\,\Sigma^+$ dipole transition intensity can be calculated by the coefficients of the Σ^+ and $\Pi^\pm$ part in each $\mathcal{L}$ component, and the coefficients of these components are obtained by diagonalizing the energy matrix of Eq. (1) for the nf complex.

A. *ns* Rydberg states (*n*=4–7)

Figures 2 and 3 shows the ion-dip spectra (upper trace) and the C(^3P) photofragment yield spectra (lower trace) for $4s\sigma(v'=0)$, $5s\sigma(v'=0)$, $6s\sigma(v'=0)$, and $7s\sigma(v'=0) \leftarrow B\,^1\Sigma^+(v''=0)$ transitions. As shown in Fig. 2, the $4s\sigma$ and $5s\sigma(v'=0) \leftarrow B\,^1\Sigma^+(v''=0)$ ion-dip spectra show two broad dips due to P and R branches, whose interval increases with J''. Actually, Komatsu *et al.*[15] reported the linewidth of the $4s\sigma$ and $5s\sigma(v'=0) \leftarrow B\,^1\Sigma^+(v''=0)$ transition to be 17 and 15 cm^{-1}, respectively. It was also found that the widths are independent of J. The results for the widths, strongly suggested that these states are subjected to predissociation.

On the other hand, the linewidth of the ion-dip spectrum of the $6s\sigma(v'=0,J')$ state appears rather sharper than that of the $4s\sigma$ and $5s\sigma(v'=0)$ states. The C(^3P) photofragment yield spectrum in Fig. 3(a) exhibits partially resolved rotational lines. Komatsu *et al.*[15] reported that the linewidth of the $6s\sigma(v'=0) \leftarrow B\,^1\Sigma^+(v''=0)$ transition to be 3.8 cm^{-1}, and the line broadening of the $ns\sigma$ states becomes smaller with the principle quantum number. They determined the potential curve of the repulsive $D'\,^1\Sigma^+$ state from the analysis of their linewidths.

In a sharp contrast to the above mentioned case, the spectra of the $7s\sigma(v'=0)$ state reproduced in Fig. 3(b) are quite different from other spectra; three rotational lines were observed in the ion-dip spectra for $J''\geqslant 1$. The spectral characteristics indicate that the spectra could not be assigned to a single transition of $7s\sigma(v'=0) \leftarrow B\,^1\Sigma^+(v''=0)$. Komatsu *et al.*[15] carried out the rotational structure analysis of these lines, and concluded that the $6d\pi(v'=0) \leftarrow B\,^1\Sigma^+(v''=0)$ transition is overlapped with the $7s\sigma(v'=0) \leftarrow B$ transition. Among three ion-dips in the Fig. 3(b), the ion-dips at the lower energy side were broader than other two ion-dips. They assigned these dips to the P branch of the $7s\sigma(v'=0) \leftarrow B(v''=0)$ transition, while the R branch of the $7s\sigma(v'=0) \leftarrow B(v''=0)$ transition was observed only at $J''=0$. The dip observed at $h\nu_3=23\,140$ cm^{-1} was assigned to

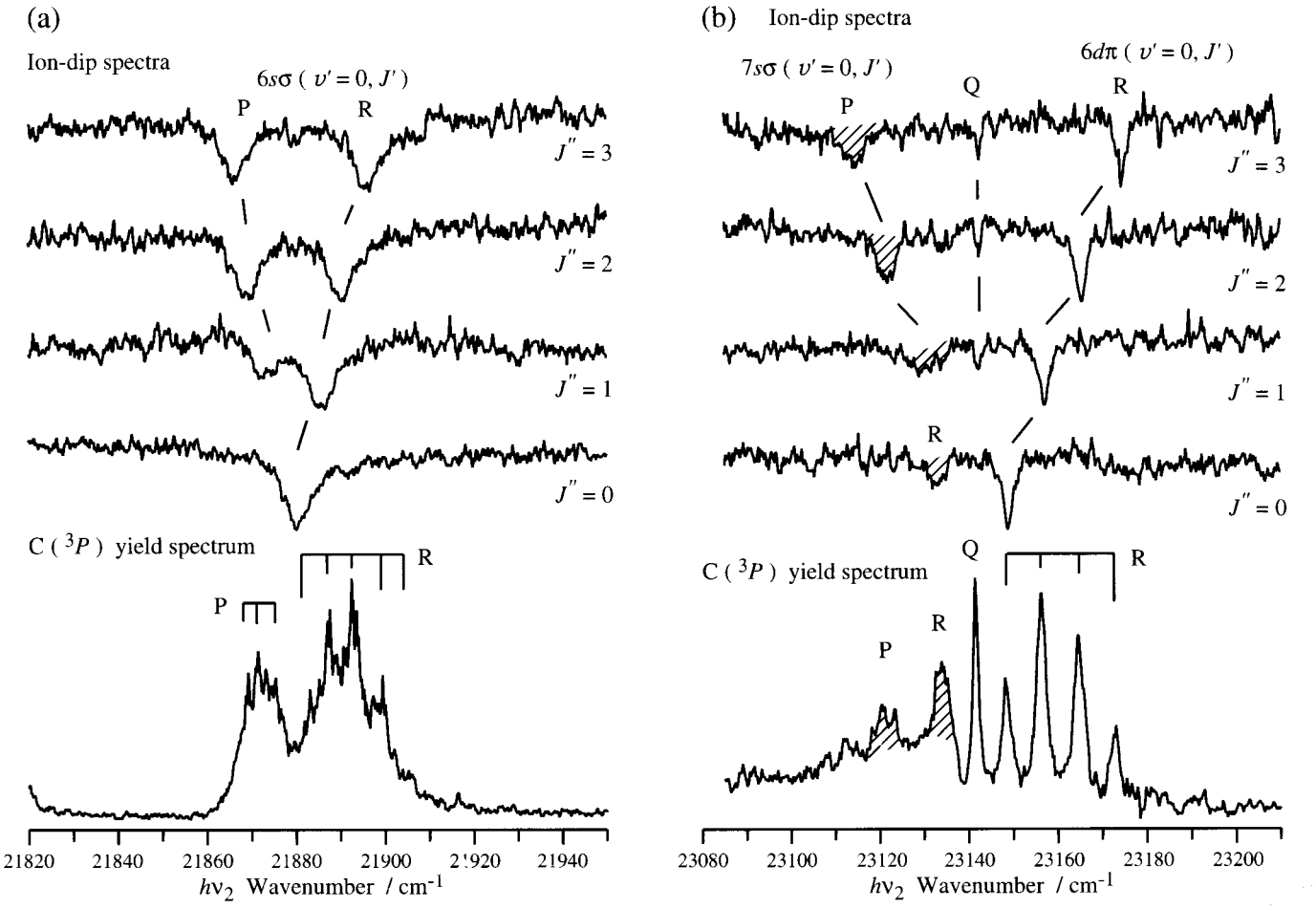

FIG. 3. $ns\sigma \leftarrow B\,^1\Sigma^+(v''=0)$ ion-dip spectra of CO (upper) and C(^3P) photofragment yield spectra (lower). (a) $6s\sigma(v'=0)$, (b) $7s\sigma(v'=0)$ and $6d\pi(v'=0)$ states. Hatched peaks were assigned to the $7s\sigma(v'=0)$ states.

the Q branches of the $6d\pi(v'=0)\leftarrow B(v''=0)$ transition. The third line in the ion-dip spectrum, which shows blue-shift with J'', was assigned to the R branches of the $6d\pi(v'=0)\leftarrow B(v''=0)$ transition. This anomalous intensity distribution was thought to be due to the $7s\sigma\,^1\Sigma^+(v'=0)\leftrightarrow 6d\pi\,^1\Pi(v'=0)$ interaction. Thus, the C(^3P) yield spectrum obtained in the present work was assigned according to their analysis. The hatched peaks in the C(^3P) yield spectrum were assigned to the P and R branches of the $7s\sigma$ state. The other peaks were assigned to the Q and R branches to the $6d\pi$ state.

B. *nd* Rydberg states ($n=3-5$)

Figure 4 shows the C(^3P) photofragment yield spectra of (a) $3d\sigma(v'=0)$, (b) $4d\sigma(v'=0)$, and (c) $5d\sigma(v'=0)\leftarrow B\,^1\Sigma^+(v''=0)$ transitions. It is noticed that the $4d\sigma(v'=0)$ spectrum exhibits well resolved branches, but the other two are broad and rotationally unresolved. The broadness of the $3d\sigma(v'=0)$ and $5d\sigma(v'=0)$ spectra is known to be due to the fast predissociation. Eidelsberg *et al.*[4,5] reported that the predissociation rates of the two states are $10^{12}\,s^{-1}$, and only the C(^3P) yield spectrum of $4d\sigma(v'=0)$ shows the sharp rotationally resolved spectrum among the $nd\sigma$ states. Eikema *et al.*,[7] who has carried out the linewidth measurements of $4d\sigma(v'=0)$, reported the predissociation rate constant up to $J=26$; the $J\leqslant 5$ levels have a constant rate of $(1.2\pm 0.2)\times 10^{11}\,s^{-1}$, and the $J=8$ and 12 levels have the largest predissociation rate constants. We also estimated the predissociation rate constant from the C(^3P) yield spectrum of Fig. 4(b). The rate constant is given by the expression $k=2\pi c\Gamma$, where Γ and c are the linewidth and the speed of light, respectively. In general, the observed linewidths are associated with not only the predissociation but also the instrumental linewidths of the laser used. It has been shown that the observed linewidth is expressed by[27]

$$\Delta\nu_L=\Delta\nu_{\rm obs}-\frac{(\Delta\nu_G)^2}{\Delta\nu_{\rm obs}}. \tag{2}$$

Here $\Delta\nu_L$, $\Delta\nu_G$, and $\Delta\nu_{\rm obs}$ are the natural (Lorentzian), laser (Gaussian), and observed linewidths, respectively. The obtained linewidth $\Delta\nu_L$ of Fig. 4(b) is 0.83 cm^{-1}, leading to the predissociation rate constant of $1.5\times 10^{11}\,s^{-1}$, which agrees very well with that of Eikema *et al.* At this stage, we do not have a reasonable explanation why the predissociation rate of the $4d\sigma$ is much slower than the $3d\sigma$ and $5d\sigma$. The difference may come from the potential crossing between the Rydberg and the dissociative state, as it was found in the

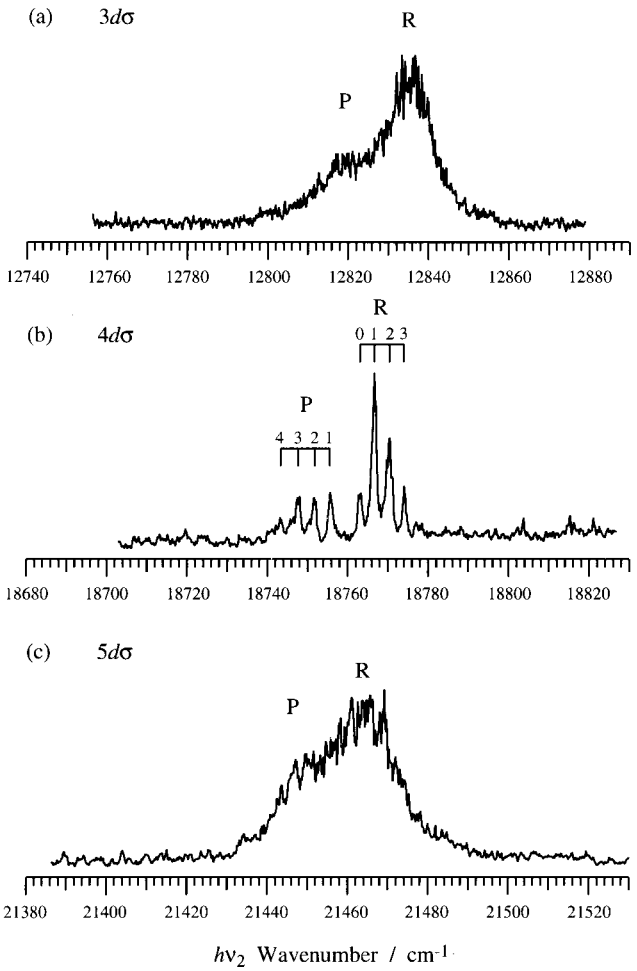

FIG. 4. $C(^3P)$ photofragment yield spectra of (a) $3d\sigma(v'=0)$, (b) $4d\sigma(v'=0)$, and (c) $5d\sigma(v'=0)\leftarrow B\,^1\Sigma^+(v''=0)$ transition.

case of the *ns* series. Further analyses for different vibrational levels are necessary to find the mechanism.

C. *np* Rydberg states (*n*=4–8)

The higher members of the *np* Rydberg series with $v=1$ were observed by Ebata *et al.*[13] for $n=8$ to $IP_{v=1}$ by using triple resonant excitation with vibrational autoionization detection. For the $v=0$ level, on the other hand, the *np* states were observed by ion-dip spectroscopy for the states up to $7p$.[15] In the present work, we examined the *np* Rydberg states by the photofragment yield spectroscopy, and carried out the rotational analysis for the $np(v=0)$ states with $n=4-8$.

Figure 5(a) shows the $C(^3P)$ photofragment yield spectrum of the $4p(v'=0)\leftarrow B\,^1\Sigma^+(v''=0)$ transition. The $4p\sigma\,K\,^1\Sigma^+$ and $4p\pi\,L\,^1\Pi$ states are observed at the total energies of 103 054 cm^{-1} ($h\nu_2=16\,138\,cm^{-1}$) and 103 271 cm^{-1} ($h\nu_2=16\,355\,cm^{-1}$), respectively. The σ and π components of the $4p$ state are well separated in this region, and the $3d\pi\,L'\,^1\Pi(v'=1)$ state is observed in the middle of the two components. The separation between the $K\,^1\Sigma^+$ and $L\,^1\Pi$ states, $C(=T_\Pi-T_\Sigma)$, is 217.2 cm^{-1}. Figure 5(b) also shows simulated spectra, which are obtained by using the rotational constants reported by Drabbels *et al.*[10] and the group of Ubachs.[7,8]

As shown in Fig. 5, the simulated spectrum of the $K\,^1\Sigma^+$ state is in good agreement with the observed, indicating that the predissociation rate of the $K\,^1\Sigma^+$ state is independent of *J*. Drabbels *et al.*[10] determined the predissociation rate constant of $K\,^1\Sigma^+$ state to be $(2.22\pm0.13)\times10^{10}\,s^{-1}$ at low *J*. In addition, Eikema *et al.*[7] reported that the predissociation rate constant is unchanged up to $J=20$.

On the other hand, the simulated $L\,^1\Pi\leftarrow B\,^1\Sigma^+$ absorption spectrum does not agree with the observed $C(^3P)$ yield spectrum, because the *Q* branch of the simulated spectrum is much stronger than that observed. The result indicates that the predissociation rate of the levels associating with the *Q* branch is expected to be much smaller than those with the *P*/*R* branches or that there exists an another dissociation channel which competes with the $C(^1D)+O(^3P)$ dissociation channel. Actually, there are two predissociation channels which are energetically possible in this energy region. That is $C(^3P)+O(^3P)$ and $C(^1D)+O(^3P)$ channels, and the latter is spin-forbidden from the $L\,^1\Pi$ state. These dissociation channels can not be discriminated from either the ion-dip measurement or the linewidth measurement. To confirm the dissociation channel, we observed the $C(^1D)$ photofrag-

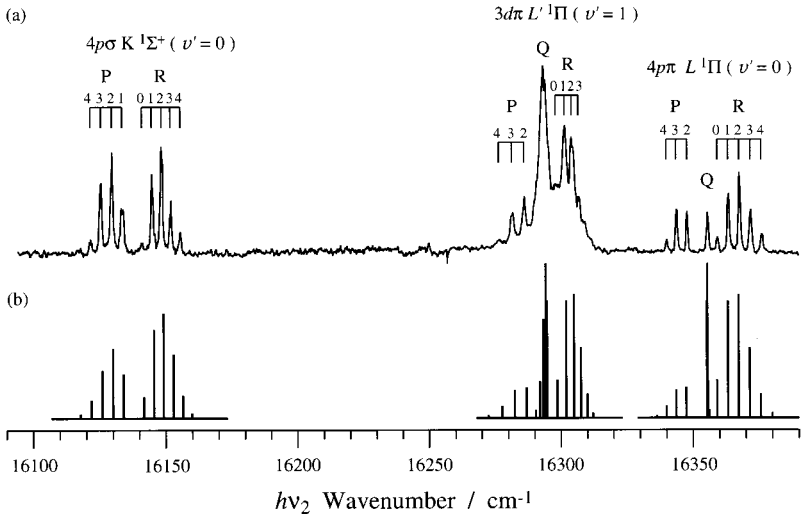

FIG. 5. (a) $C(^3P)$ photofragment yield spectrum and (b) simulated absorption spectrum of the $4p\sigma\,K\,^1\Sigma^+(v'=0)$, $3d\pi\,L'\,^1\Pi(v'=1)$, and $4p\pi\,L\,^1\Pi(v'=0)\leftarrow B\,^1\Sigma^+(v''=0)$ transition.

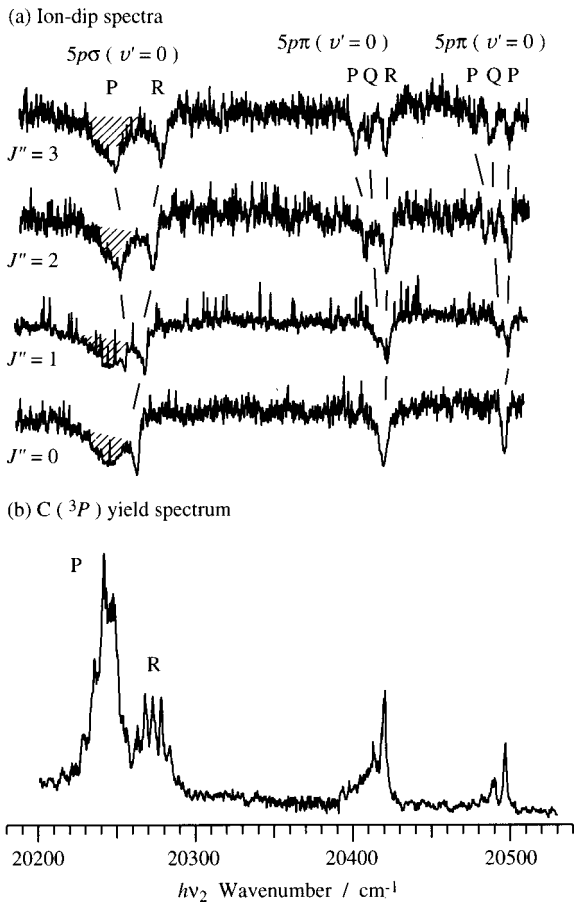

FIG. 6. (a) ion-dip spectra and (b) C(^3P) photofragment yield spectrum of the $5p\pi(v'=0)$ and $5p\sigma(v'=0)\leftarrow B\,^1\Sigma^+(v''=0)$ transition. Hatched peaks in the ion-dip spectra belong to unidentified transition of CO (see text).

ment and its yield spectrum, which will be discussed in the next section.

Figure 6(b) shows the C(^3P) photofragment yield spectrum of the $5p(v'=0,J')\leftarrow B\,^1\Sigma^+(v''=0,J'')$ transition, being compared with the ion-dip spectra [Fig. 6(a)]. The $5p\sigma(v'=0)$ state is observed at the total energy of 107 174 cm^{-1} ($h\nu_2=20\,258\,cm^{-1}$). In the $5p\sigma\,^1\Sigma^+(v'=0)\leftarrow B\,^1\Sigma^+(v''=0)$ C(^3P) yield spectrum, it is seen that the *P* branch is broader and much stronger than the *R* branch. This anomalous intensity of the *P* branch can be understood by comparing the ion-dip spectra. As seen in Fig. 6(a), a broad peak is observed at $h\nu_2\sim 20\,240\,cm^{-1}$ in the ion-dip spectrum, which locates at 20 cm^{-1} to the lower frequency side of the *R* branch. This broad peak is observed even in the transition from the $J''=0$ level of the *B* state, indicating that the broad state has the $^1\Pi$ character. Thus, the overlapping of the broad band makes the *P* branch stronger than the *R* branch. Eikema *et al.*[7] reported the predissociation rate of $5p\sigma$ to be $(3.4\pm2.0)\times10^{10}\,s^{-1}$ for $J=0$ and $(1.8\pm0.5)\times10^{11}\,s^{-1}$ for $J=1$. This *J*-dependence indicates that the predissociation occurs via heterogeneous perturbation through the repulsive $^1\Pi$ state.

In the region of the $5p\pi(v'=0)\leftarrow B\,^1\Sigma^+(v''=0)$ transition, two $^1\Pi\leftarrow{}^1\Sigma^+$ transitions are observed at the total energy region of 107 340 and 107 420 cm^{-1}, which corresponds to $h\nu_2$ of 20 420 and 20 500 cm^{-1}. Komatsu *et al.*[15] has carried out the rotational structure analysis of these lines, and reported that $B'=1.37\,cm^{-1}$ for the lower energy state and $B'=1.57\,cm^{-1}$ for the upper state, which are much smaller than that of the *B* state ($B''=1.94\,cm^{-1}$). As seen in Fig. 6(a), the *P*, *Q*, and *R* branches shift to red with the increase of *J* in both states. In the C(^3P) yield spectrum, the peaks at the $h\nu_2=20\,420$ and 20 497 cm^{-1} were assigned to the *R* heads, and the *P* and *Q* branches are overlapped in the red side. Eikema *et al.*[7] reported the predissociation rate constant of $5p\pi$ to be $k_p>3\times10^{11}\,s^{-1}$ for the higher energy state and $k_p=2.7\times10^{11}\,s^{-1}$ for the lower state. They also reported that the predissociation rate constant of the lower energy states was independent of *J*. Though they observed a sharp $^1\Sigma^+$ state in the region between the two $^1\Pi$ states, we could not observe the state either in the ion-dip spectra or the photofragment yield spectrum, and the existence of the $^1\Sigma^+$ state remains unclear.

Figure 7 shows the C(^3P) yield spectra of the (a) $6p(v'=0)$, (b) $7p(v'=0)$, and (c) $8p(v'=0)\leftarrow B\,^1\Sigma^+(v''=0)$ transitions. The $p\sigma-p\pi$ energy separations of the $6p$ and $7p$ states are reported to be 35.8 and 52.0 cm^{-1} by Komatsu *et al.*,[15] and we simulated the spectra for the $6p$, $7p(v'=0)\leftarrow B\,^1\Sigma^+(v''=0)$ transitions by using those values. For the $8p(v'=0)$, we determined the $p\sigma-p\pi$ energy separation to be 16.4 cm^{-1} by fitting the simulated spectrum to the observed one. Different from the *np* Rydberg states with $n\leqslant5$, the $6-8p$ states are switched into Hund's case (d), and the calculation of the rotational structures was carried out by the *l*-uncoupling Hamiltonian of Eq. (1). The simulated absorption spectra of these *np* states are illustrated in the lower part of Fig. 7, in which the rotational branches are labeled by the $^{N^{+\prime}-N''}\Delta J_{\mathcal{L}'}$ expression. Different from the $4p$ state, the calculated spectra reproduce very well the observed ones and the predissociation rates of these *np* states are independent of *J* and the *e*/*f* parity. These results suggest that both the $2\,^1\Pi$ and the $D'\,^1\Sigma^+$ repulsive states are acting as the dissociative states, which correlate to the C(^3P)+O(^3P) channel.

D. $4p\pi\,L\,^1\Pi(v'=0)$, and $3d\pi\,L'\,^1\Pi(v'=1)$ Rydberg states

In order to investigate the dissociation pathways of $4p\pi\,L\,^1\Pi(v'=0)$ in detail, we analyzed the C(^3P,^1D) and O(^3P) photofragments generated from the state. The generation of the C(^1D) fragment provides a direct evidence of the dissociation to the C(^1D)+O(^3P) channel. Since the O(^3P) is the common product for the C(^3P)+O(^3P) and the C(^1D)+O(^3P) channels, the O(^3P) yield spectrum provides us with the overall dissociation yield irrespective to the channel. Figure 8 shows the C(^3P), C(^1D), and O(^3P) photofragment yield spectra of the $L\,^1\Pi(v'=0)$ and $L'\,^1\Pi(v'=1)\leftarrow B\,^1\Sigma^+(v''=0)$ transitions. As seen in Figs. 8(a) and 8(b), the relative intensity of the *Q* branch to the *P* or *R* branch of the C(^3P) and C(^1D) yield spectra for the $L\,^1\Pi(v'=0)$ state are quite different with each other; the *Q* branch is weaker than the *P* and *R* branches in the C(^3P) yield spectrum and the reverse is seen in the C(^1D) yield

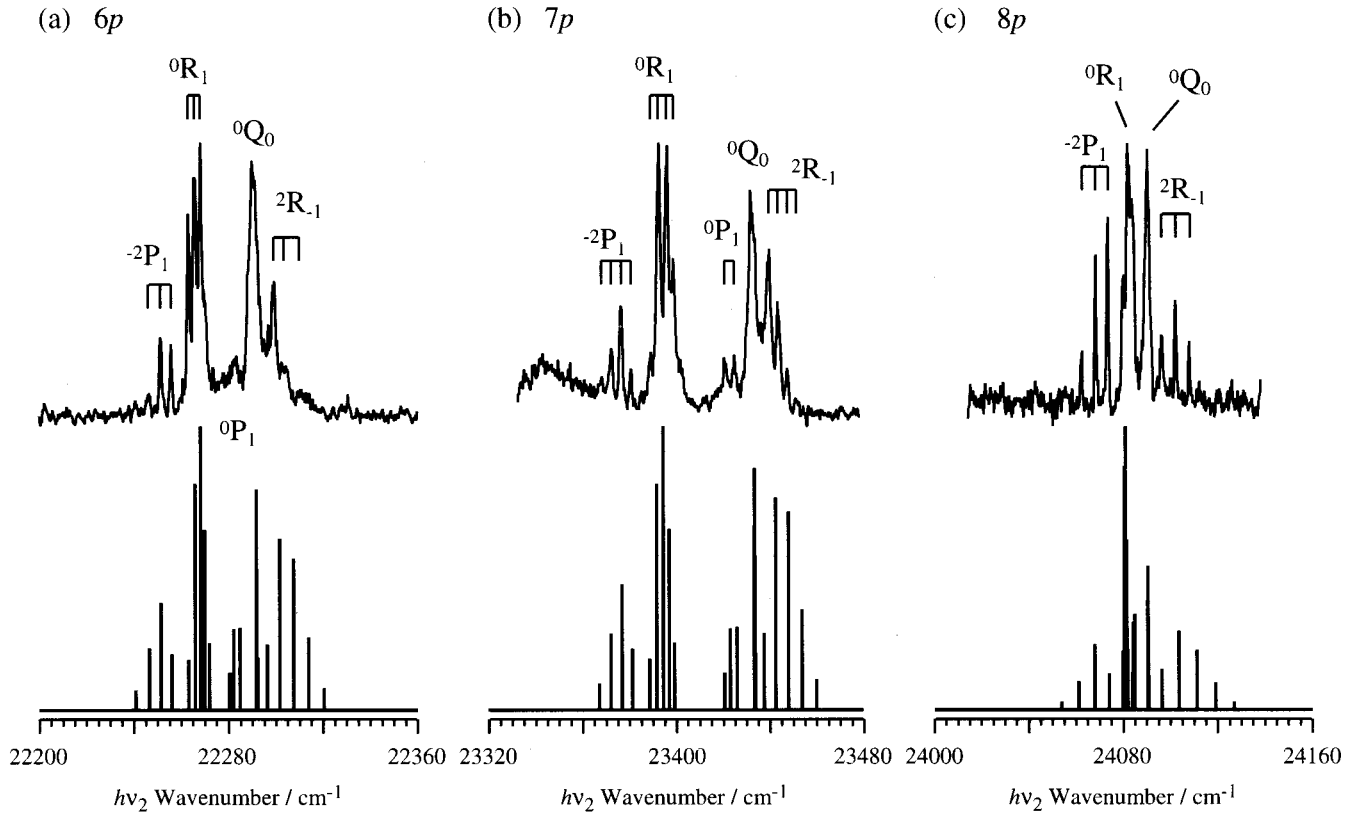

FIG. 7. (Upper) C(^3P) photofragment yield spectra and (lower) simulated absorption spectra of the (a) $6p(v'=0)$, (b) $7p(v'=0)$, and (c) $8p(v'=0)$ $\leftarrow B\,^1\Sigma^+(v''=0)$ transition.

spectrum. Figure 8(d) shows the simulated $^1\Pi\leftarrow{}^1\Sigma^+$ spectrum, which is convoluted from Fig. 5(b) by using the reported linewidth.[10] As was described above, the O(^3P) is the common product for the two channels and the simulated $^1\Pi\leftarrow{}^1\Sigma^+$ spectrum of Fig. 8(d) well reproduces the O(^3P) yield spectrum of Fig. 8(c).

The disagreement of the observed C(^3P) and C(^1D) fragment yield spectra with the simulated one can be explained by assuming that the branching ratio of the two channels depends on the parity and J of the $L\,^1\Pi(v'=0)$ state. In the $^1\Pi\leftarrow{}^1\Sigma^+$ transition, the upper levels of the Q branch belong to the f-symmetry and those of the P and R branches to the e-symmetry. So, we tried to reproduce the observed photofragment yield spectra of Figs. 8(a) and 8(b) by using different dissociation rate constants for the different symmetry (or parity) components to the two dissociation channels. In this process we used the total dissociation rate constant ($k=k_S+k_T$) to be the value reported by Drabbels *et al.*[10] The predissociation rate constant for the e-symmetry component is expressed by a sum of the J-independent and dependent terms, as expressed as follows:

$$k^e=k_0+k_J J(J+1). \tag{3}$$

On the other hand, the predissociation rate constant for the f-symmetry component is expressed by a J-independent term,

$$k^f=k_0. \tag{4}$$

For the spin-forbidden channel, we assumed that the dissociation rate constant is J-independent, since the spin–orbit coupling does not include the J-dependent term. Thus, k_0 is the sum of the two channels, that is,

$$k_0=k_0^S+k_0^T. \tag{5}$$

The intensities of each channel are given by

$$I(\mathrm{C}(^3P))=S_{J'J''}\times\frac{k_S}{k_S+k_T}, \tag{6}$$

and

$$I(\mathrm{C}(^1D))=S_{J'J''}\times\frac{k_T}{k_S+k_T}, \tag{7}$$

where $S_{J'J''}$ is the $L\,^1\Pi(v'=0)\leftarrow B\,^1\Sigma^+(v''=0)$ transition intensity. Drabbels *et al.* reported that $k_0=1.9\times10^9\ \mathrm{s}^{-1}$ and $k_J=1.2\times10^9\ \mathrm{s}^{-1}$. By changing the k_0^T as a parameter, we obtained the best fitting of all photofragment yield spectra, when we assumed $k_0^S=0.5\times10^9\ \mathrm{s}^{-1}$ and $k_0^T=1.4\times10^9\ \mathrm{s}^{-1}$. The insets in Figs. 8(a) and 8(b) show the simulated spectra by using Eqs. (6) and (7), and the simulated spectra well reproduced the observed ones. It shows that the predissociation of the $L\,^1\Pi(v'=0)$ state to the spin-forbidden channel competes with that to the spin-allowed channel with the comparable rate constant.

The $L'\,^1\Pi(v'=1)\leftarrow B\,^1\Sigma^+(v''=0)$ transition is observed at the total energy of 103 211 cm^{-1} ($h\nu_2$

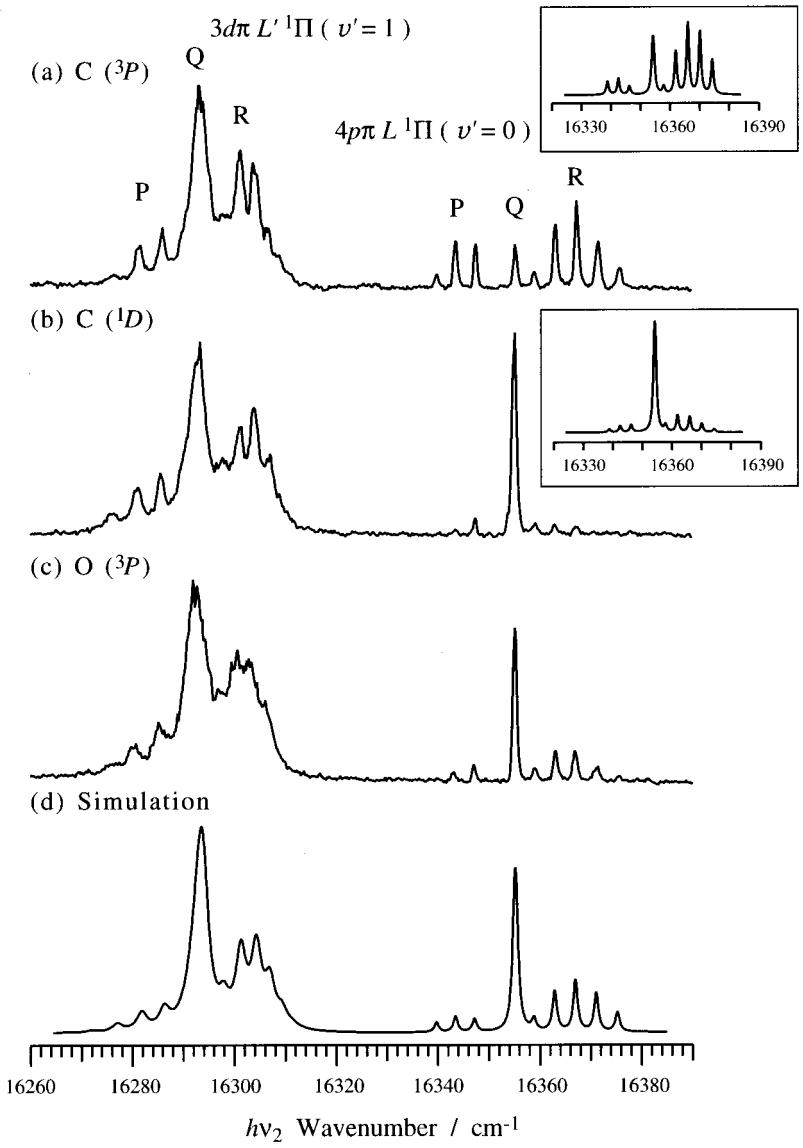

FIG. 8. Photofragment yield spectra of the $3d\pi\, L'\,^1\Pi(v'=1)$ and $4p\pi\,^1\Pi(v'=0)\leftarrow B\,^1\Sigma^+(v''=0)$ transitions observed by (a) C(^3P), (b) C(^1D), and O(^3P) photofragments. (d) Simulated absorption spectrum of $L'\,^1\Pi(v'=1)$ and $L\,^1\Pi(v'=0)\leftarrow B\,^1\Sigma^+(v''=0)$ transitions. The insets in (a) and (b) show the simulated spectra by including the C(^3P,^1D) yield (see text).

$=16\,295\,\mathrm{cm}^{-1}$). Though the $L'\,^1\Pi(v'=1)$ and $L\,^1\Pi(v'=0)$ states are separated by only 60 cm^{-1}, they are quite different with respect to the rotational structures and the linewidths. First, the reported rotational constant $B=1.7966\,\mathrm{cm}^{-1}$ of $L'\,^1\Pi(v'=1)$ is much smaller than that of $L\,^1\Pi(v'=0)$ ($B=1.9796\,\mathrm{cm}^{-1}$).[5] Second, as illustrated in Fig. 8(d), the relative intensities of the C(^3P) and C(^1D) yield spectra agree with the simulated spectrum, in which neither *J*- nor parity-dependence is assumed. We tried to estimate the branching ratio to the C(^3P) and C(^1D) channels for the $L'\,^1\Pi(v'=1)$ state from the relative intensities of the rotational branches between the $L'\,^1\Pi(v'=1)$ and the $L\,^1\Pi(v'=0)$ states. In the C(^3P) and C(^1D) yield spectra, the observed photofragment intensities, $I(\mathrm{C}(^3P))$ and $I(\mathrm{C}(^1D))$, of $L\,^1\Pi(v'=0)$ are expressed by

$$I(\mathrm{C}(^3P))=A_1\sigma I\phi_{4p\pi}, \tag{8}$$

$$I(\mathrm{C}(^1D))=A_2\sigma I\phi'_{4p\pi}. \tag{9}$$

Here, σ is the absorption cross section of the $L\,^1\Pi(v'=0)\leftarrow B\,^1\Sigma^+(v''=0)$ transition, I is the ν_2 power. A_1 and A_2 are the detection efficiencies of the C(^3P) and C(^1D) atomic fragments, $\phi_{4p\pi}$ and $\phi'_{4p\pi}$ are the dissociative quantum yields of the C(^3P) and C(^1D) channels for $L\,^1\Pi(v'=0)$, respectively. The C(^3P)/C(^1D) branching ratio for $L\,^1\Pi(v'=0)$ is expressed by $\phi_{4p\pi}/\phi'_{4p\pi}$, which is equal to k_0^S/k_0^T for the *f*-symmetry component. So, we compared the *Q* branch intensity of the C(^3P) yield spectrum with that of the C(^1D) yield spectrum. The *Q* branch intensity ratio has the following relation:

$$\frac{I(\mathrm{C}(^3P))}{I(\mathrm{C}(^1D))}=\frac{A_1\sigma I\phi_{4p\pi}}{A_2\sigma I\phi'_{4p\pi}}=\frac{A_1k_0^S}{A_2k_0^T}. \tag{10}$$

Similarly, in the case of the $L'\,^1\Pi(v'=1)$ dissociation, the intensity ratio of the *Q* branch is given by

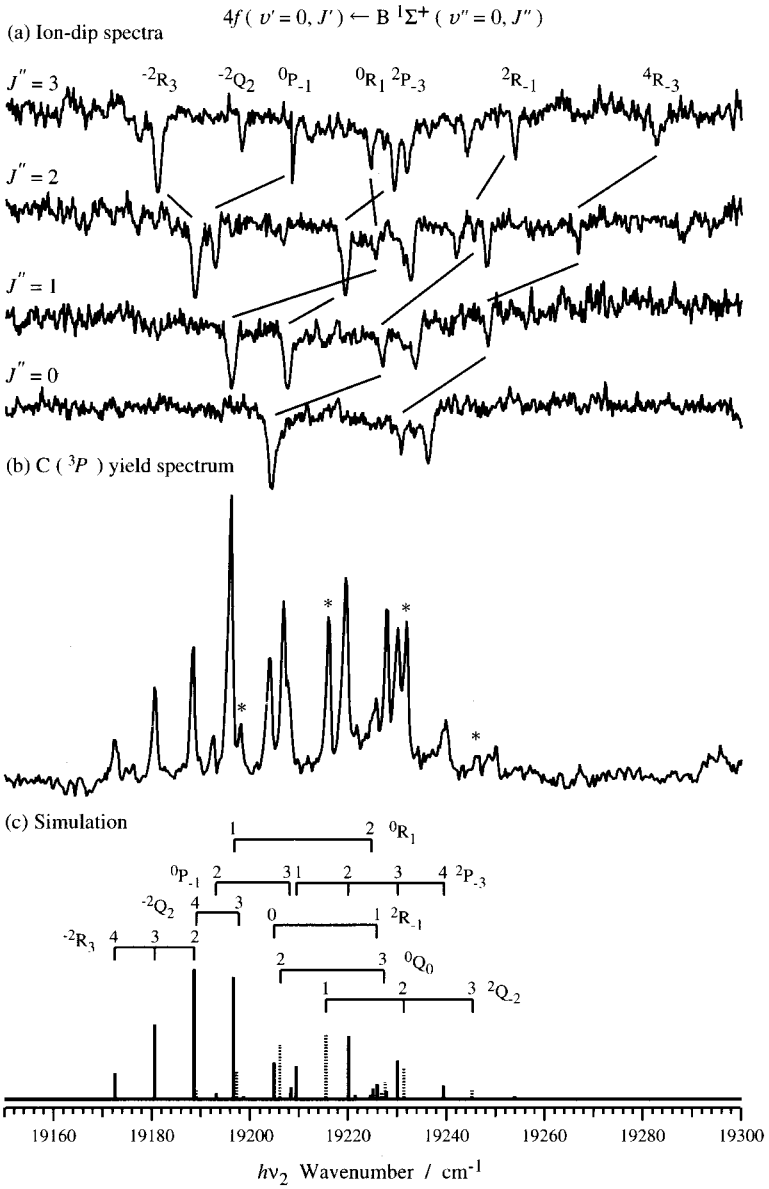

FIG. 9. (a) Ion-dip spectra, (b) C(^3P) photofragment yield spectrum, and (c) simulated absorption spectrum of the $4f(v'=0)\leftarrow B\,^1\Sigma^+(v''=0)$ transition. The peaks marked by asterisks in the C(^3P) yield spectrum are assigned to Q branches (see text).

$$\frac{I'(\mathrm{C}(^3P))}{I'(\mathrm{C}(^1D))}=\frac{A_1\sigma' I\phi_{3d\pi}}{A_2\sigma' I\phi'_{3d\pi}}=\frac{A_1 k_0^{S'}}{A_2 k_0^{T'}}. \tag{11}$$

Here, σ' is the absorption cross section of the $L'\,^1\Pi(v'=1)\leftarrow B\,^1\Sigma^+(v''=0)$ transition, $\phi_{3d\pi}$ and $\phi'_{3d\pi}$ are the dissociative quantum yields, $k_0^{S'}$ and $k_0^{T'}$ are the predissociation rate constants of C(^3P) and C(^1D) channels for $L'\,^1\Pi(v'=1)$, respectively. The intensity ratio of $L'\,^1\Pi(v'=1)$ is also expressed by that of $L\,^1\Pi(v'=0)$ with the following relations:

$$\frac{I'(\mathrm{C}(^3P))}{I'(\mathrm{C}(^1D))}=\frac{I'(\mathrm{C}(^3P))}{I(\mathrm{C}(^3P))}\frac{I(\mathrm{C}(^3P))}{I'(\mathrm{C}(^1D))}$$

$$=\frac{I'(\mathrm{C}(^3P))}{I(\mathrm{C}(^3P))}\frac{I(\mathrm{C}(^1D))}{I'(\mathrm{C}(^1D))}\frac{A_1 k_0^S}{A_2 k_0^T}. \tag{12}$$

Here, Eq. (10) is used in the second step. In Eq. (12), the ratio $I'(\mathrm{C}(^3P))/I(\mathrm{C}(^3P))$ and $I(\mathrm{C}(^1D))/I'(\mathrm{C}(^1D))$ are obtained to be 4.0 and 1.0, respectively, by comparing the Q branch intensities of the C(^3P) yield and C(^1D) yield spectra for the $L'\,^1\Pi(v'=1)$ and the $L\,^1\Pi(v'=0)$ states of Figs. 8(a) and 8(b). Finally, from the result of Eqs. (11) and (12), the branching ratio of C(^3P) to C(^1D) of $L'\,^1\Pi(v'=1)$ is obtained,

$$\frac{k_0^{S'}}{k_0^{T'}}=\frac{4.0k_0^S}{k_0^T}, \tag{13}$$

where k_0^S/k_0^T is already obtained to be 1.4. The total predissociation rate of $L'\,^1\Pi(v'=1)$ is obtained to be $k_0^{S'}+k_0^{T'}=(2.7\pm0.9)\times10^{11}\,\mathrm{s}^{-1}$, from the rotational linewidth measurements,[7] and the estimated predissociation rate constants to the C(^3P) and C(^1D) channels of $L'\,^1\Pi(v'=1)$ are $1.6\times10^{11}\,\mathrm{s}^{-1}$ and $1.1\times10^{11}\,\mathrm{s}^{-1}$, respectively.

Though the reason of such a large difference of the predissociation rate constants between the two states is still unclear, either the difference in the vibrational quantum number or in the angular momentum of the Rydberg orbital

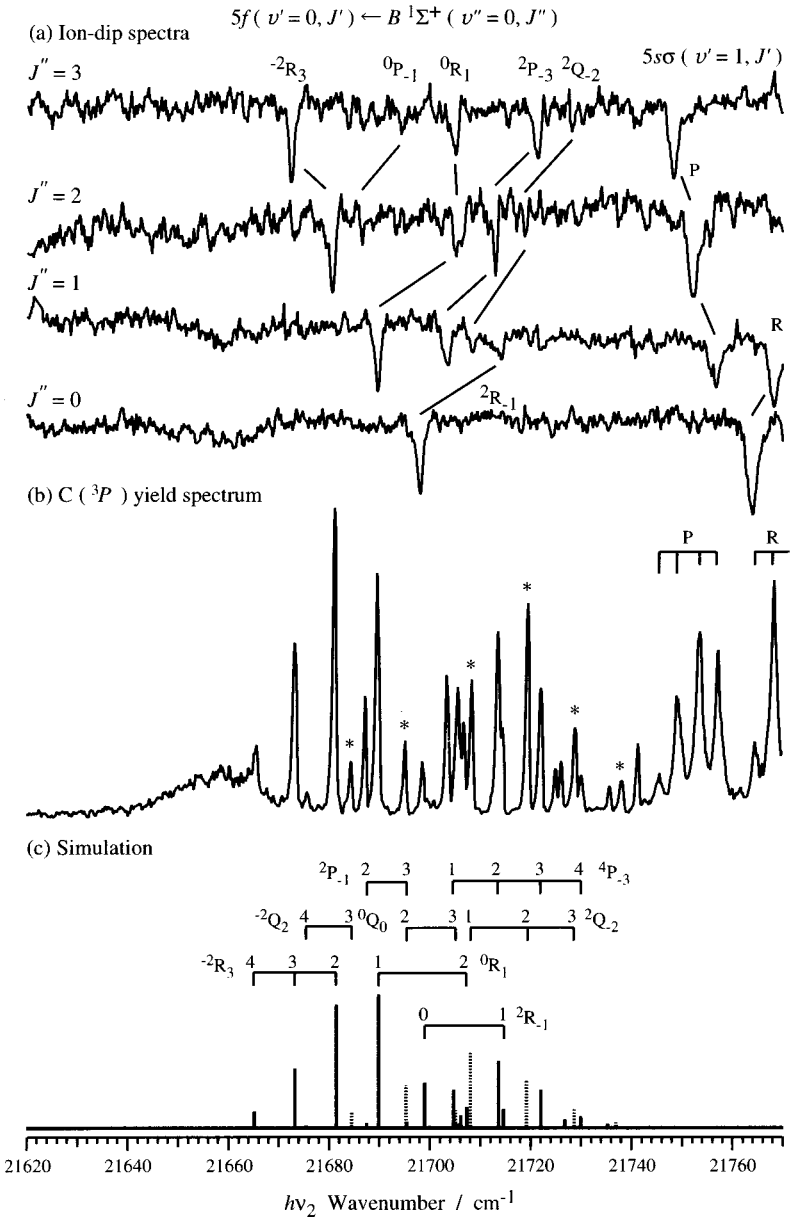

FIG. 10. (a) Ion-dip spectra, (b) C(^3P) photofragment yield spectrum, and (c) simulated absorption spectrum of the $5f(v'=0)\leftarrow B\,^1\Sigma^+(v''=0)$ transition. The peaks marked by asterisks in the C(^3P) yield spectrum are assigned to Q branches (see text).

might be responsible. As to the repulsive valence states, O'Neil and Schaefer[28] calculated potential curves of the valence states with the different spin manifold. Among them, it is seen that the $3\,^3\Pi$ and $2\,^3\Sigma^-$ states, both of which correlate to the $C(^1D)+O(^3P)$ channel, are crossing at the bottom of the potential curves of the Rydberg states. Therefore, these states are candidates for the dissociative states. To find more information of the repulsive state, we tried to detect $C(^1D)$ fragment at higher Rydberg states with different vibrational levels. However, we could not detect the $C(^1D)$ fragment from other Rydberg states, indicating only the $L'\,^1\Pi(v'=1)$ and the $L\,^1\Pi(v'=0)$ are strongly coupled to the spin-forbidden $C(^1D)+O(^3P)$ channel.

E. *nf* Rydberg states ($n=4-7$)

The rotational analysis of the $v=0$ level of the $4f-6f$ states was first carried out by Komatsu *et al.*[15] They reported that the long range force model reproduces well the term values of the nf states, and determined the ionization potential of the $v=0$ level. In addition, they suggested that the predissociation rate constants of the *e*-symmetry levels are much larger than those of the *f*-symmetry levels. They concluded that the predissociation of the nf state occurs via the $D'\,^1\Sigma^+$ state which perturbs only the *e*-symmetry component of the $v=0$ level. In the present work, we observed the $nf(v'=0)\leftarrow B\,^1\Sigma^+(v''=0)$ transition by the $C(^3P)$ yield spectroscopy and compared the spectra with the simulated ones by using *l*-uncoupling model, Eq. (1).

Figure 9(a) shows the ion-dip and 9(b) the $C(^3P)$ photofragment yield spectra of the $4f(v'=0)\leftarrow B\,^1\Sigma^+(v''=0)$ transition. Figure 9(c) shows the simulated rotational structure with solid lines for the *e*-symmetry component and dotted lines for the *f*-symmetry one. The spectrum in Fig. 9(c) was simulated by using $T_\Sigma=106\,107\,\mathrm{cm}^{-1}$ and $C=5.7\,\mathrm{cm}^{-1}$, which were determined by Komatsu *et al.*[15] The rotational branches are labeled by ${}^{N^{+\prime}-N''}\Delta J_{\mathcal{L}'}$ and the as-

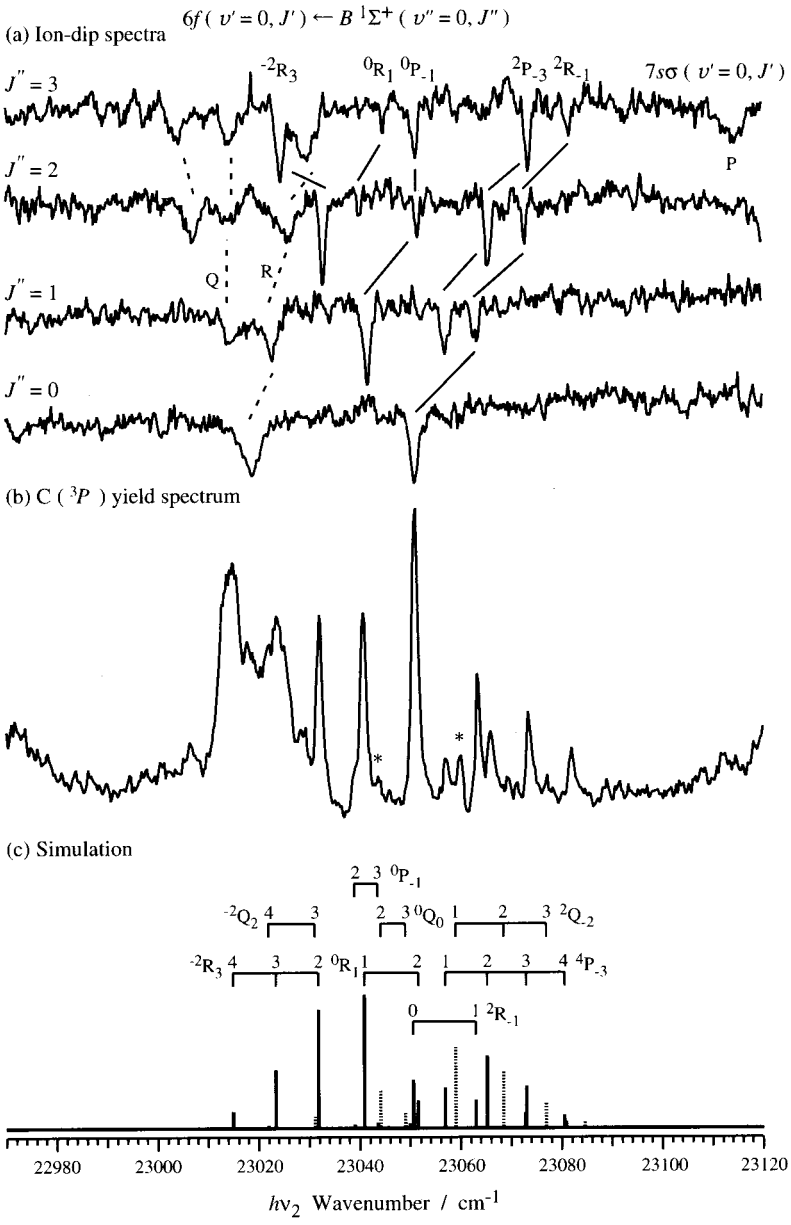

FIG. 11. (a) Ion-dip spectra, (b) C(^3P) photofragment yield spectrum, and (c) simulated absorption spectrum of the $6f(v'=0) \leftarrow B\,^1\Sigma^+(v''=0)$ transition. The peaks marked by asterisks in the C(^3P) yield spectrum are assigned to Q branches (see text).

signment are shown in the figure. The simulated rotational structures reproduce the observed C(^3P) yield spectrum well, while the intensity in higher ν_2 region is slightly different because of the overlapped transitions of different electronic states. In Fig. 9, a difference between the ion-dip spectrum and the C(^3P) yield spectrum is apparent, since the $^{-2}Q_2$, $^0Q_0$, and $^2Q_{-2}$ branches marked by asterisks appear to be intense in the C(^3P) yield spectrum. As seen in Fig. 9(a), since only the P and R branches (e-symmetry components) are strongly observed in the ion-dip spectra, Komatsu *et al.* suggested that only the e-symmetry components selectively predissociate. Based on the selection rule for the perturbation, $\Delta J=0$ and $\pm \leftrightarrow \pm$, they reported the $4f$ state predissociates to the $D'\,^1\Sigma^+$ state. In the C(^3P) fragment spectrum of Fig. 9(b), however, Q branches (f-symmetry components) are observed with comparable intensities to other branches. Thus, it is concluded that the f-symmetry levels are also subject to dissociate in $4f(v'=0)$. The difference of the relative intensities between the ion-dip and the C(^3P) yield spectra can be interpreted on the basis of the nature of the ion-dip spectra; the dip intensity is proportional to the product of the $nf \leftarrow B\,^1\Sigma^+$ transition intensity and the predissociation rate of the upper state. If the predissociation rate of the nf Rydberg state is small, CO molecules pumped to the Rydberg state with the intense ν_1 laser (300 μJ) are ionized by absorbing additional photons prior to the predissociation. In such a case the dip becomes weak or disappears. In the photofragment yield spectroscopy, on the other hand, the intensities of ν_1 (30 μJ) and ν_2 (50 μJ) are adjusted to be very weak, so that the dissociation rate is expected to be much larger than the ionization rate. Thus, the C(^3P) fragments are detected even if the dissociation rate is small. These results lead to the conclusion that in the $4f(v'=0)$ Rydberg state, both the e- and f-symmetry components predissociate and the rate of the e-symmetry is larger than that of the f-symmetry components, in agreement with Komatsu *et al.*

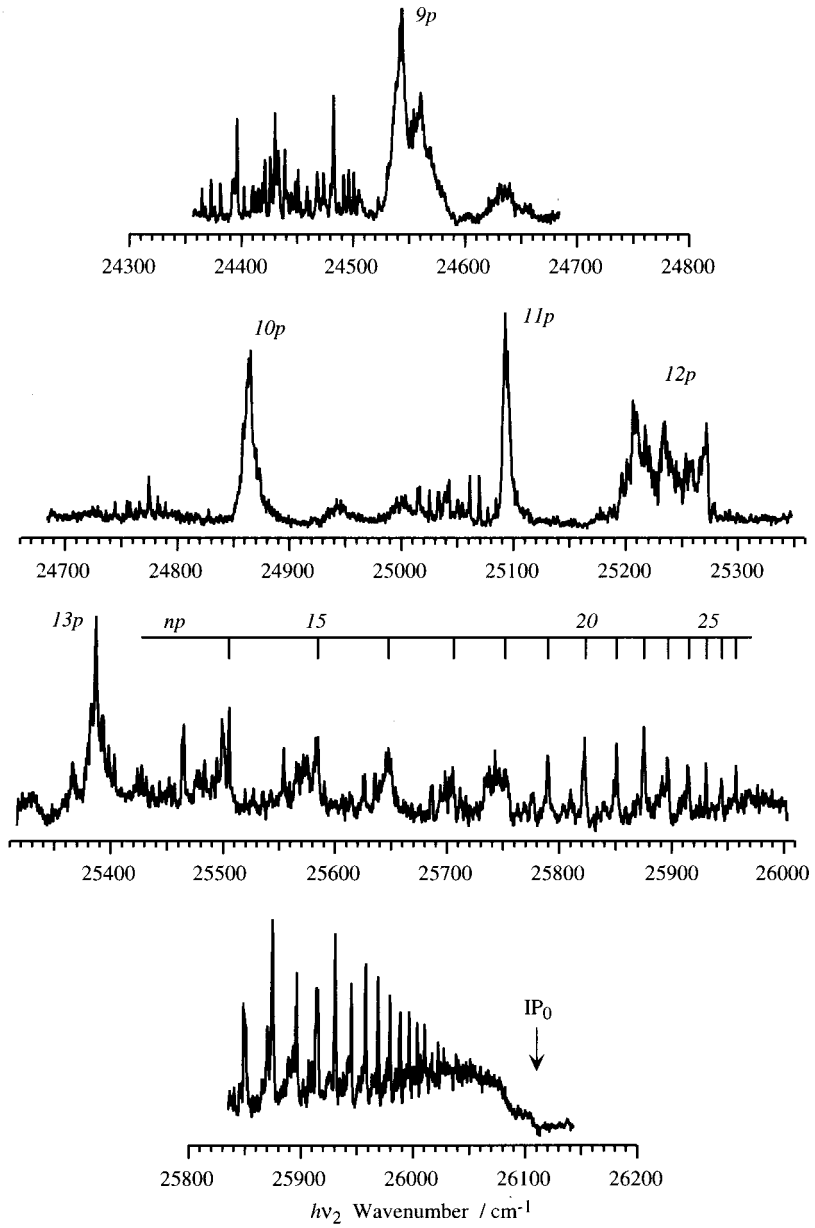

FIG. 12. C(^3P) photofragment yield spectra of CO($v'=0$) in the energy region from $9p$ state to ionization threshold, IP_0.

Figure 10 shows (a) the ion-dip and (b) the C(^3P) yield spectra of the $5f$ states. The spectral simulation was carried out by the same procedure as the $4f$ state, which is shown in Fig. 10(c). The values of $T_\Sigma = 108\,601\,\mathrm{cm}^{-1}$ and $C = 3.7\,\mathrm{cm}^{-1}$ were used for the simulation. As shown in the figure, the simulated spectrum reproduces the observed C(^3P) yield spectrum similar to the $4f(v'=0)$ state. Similar to the case of the $4f$ state, it is seen that the $^{-2}Q_2$, $^0Q_0$, and $^2Q_{-2}$ branches [marked by an asterisks in the C(^3P) yield spectrum] are missing in the ion-dip spectra. Thus, it is also concluded that the *e*-symmetry components dissociate faster than that of the *f*-symmetry.

At $h\nu \sim 21\,760\,\mathrm{cm}^{-1}$, the *P* branches of the $5s\sigma(v'=1)$ state are overlapped with the $5f(v'=0)$ state. As seen in the figure, the linewidths of the $5f$ state are sharper than those of $5s\sigma(v'=1)$, whose predissociation rate constant was estimated to be $k_p = 3.7\times 10^{11}\,\mathrm{s}^{-1}$.[15] It shows that the the predissociation rate constant of the $5f$ state is smaller than that of the $5s\sigma(v'=1)$ state.

Figure 11(a) shows the ion-dip and 11(b) the C(^3P) yield spectra of the $6f(v'=0)$. Simulated spectrum are shown in Fig. 11(c), for which the values of $T_\Sigma = 109\,957\,\mathrm{cm}^{-1}$ and $C = 1.6\,\mathrm{cm}^{-1}$ were used. At $h\nu_2 \sim 23\,020\,\mathrm{cm}^{-1}$, broad bands are overlapped with the $^{-2}R_3$ branches in both the ion-dip and the C(^3P) yield spectra. In the ion-dip spectra, the *P* and *R* branches (*e*-symmetry components) dominate, while the *Q* branches are completely missing. In contrast, the *Q* branches were observed very weak in the C(^3P) yield spectrum. As seen in the calculated spectrum of Fig. 11(c), on the other hand, the intensities of $^0Q_0$ and $^2Q_{-2}$ branches are comparable to the *P* and *R* branches. Thus, different from the $4f$ and $5f$ states, the predissociation of the *e*-symmetry component is more dominant than that of the *f*-symmetry component in the $6f(v'=0)$

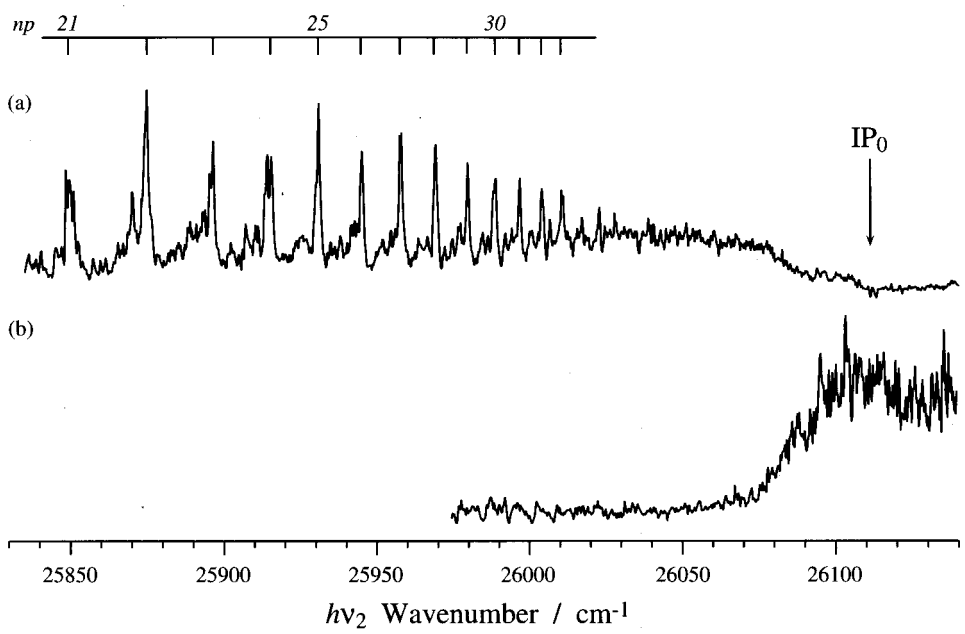

FIG. 13. (a) C(^3P) photofragment yield spectrum and (b) two-color ionization spectrum of CO in the energy region from the 21p state to ionization threshold.

state, indicating that the interaction of the $6f(v'=0)$ state with the $D'\,^1\Sigma^+$ valence state is much stronger than the $4f(v'=0)$ and $5f(v'=0)$ states.

F. Higher Rydberg series converging to the ionization limit

Figure 12 shows the C(^3P) yield spectra in the energy region from $9p(v'=0)$ to ionization threshold, IP_0. In the figure, almost all the bands are assigned to the Rydberg series converging to the adiabatic ionization energy, IP_0. Among them, the np series are clearly identified up to $n \approx 30$. Since the intermediate state is fixed to the $3s\sigma\,B\,^1\Sigma^+(v''=0)$ state, the $v'=0$ levels of the np states may predominantly appear because of the atomic like selection rule of $\Delta l=\pm 1$ and the propensity rule of $\Delta v=0$ for the Rydberg–Rydberg transition. In general, the linewidth of the high Rydberg state becomes sharper at larger n due to the reduction of the interaction between the repulsive valence state and the Rydberg orbitals, and also due to the strong $\Delta(R'-N'')=0$ rotational transition at high Rydberg state.[29] However, the observed rotational spectrum of each Rydberg state is not as simple as seen in the figure. For example, 12p and $14p \sim 18p(v'=0)$ series show complicated rotational structures, and the linewidth of $9p(v'=0)$ is much broader than that of $8p(v'=0)$ [Fig. 7(c)]. The broadness of 9p may be attributed to a large predissociation rate constant for this state, and the similar feature was also seen in the $9p(v'=1)$ level.[13] One of the possibilities of such a large predissociation in this region is due to opening of an additional dissociation channel, since the dissociation threshold of the $C(^1D)+O(^1D)$ channel is 111 029 cm^{-1} corresponding to $\nu_2 \sim 24\,133\,cm^{-1}$. Actually, Rosen *et al.*[30] observed the $C(^1D)+O(^1D)$ channel by using the dissociative recombination between an electron and CO^+. Thus, the detection of the $O(^1D)$ atom is also important for the investigation of the predissociation mechanism of higher Rydberg states of CO.

As seen in the lowest trace of Fig. 12, the intensity of the C(^3P) yield spectrum suddenly drops above $\nu_2 \sim 26\,080\,cm^{-1}$, which is ~ 30 cm^{-1} lower than IP_0 at 113 025 cm^{-1} ($h\nu_2 = 26\,109\,cm^{-1}$). This sudden drop was found to be due to the field ionization by an external electric field. The decrease of IP by the external field is expressed as follows:[31,32]

$$\Delta = \alpha F^{1/2}. \tag{14}$$

Here, Δ is the shift of the ionization potential and F is the external electric field strength and α is given to be -4 $cm^{-1}/(V/cm)^{1/2}$ by calculating a purely Coulombic potential. Figure 13 shows a comparison of the C(^3P) yield spectrum and the two-color ionization spectrum of CO^+ in the IP_0 region, which was observed at the applied field strength of 70 V/cm. The CO^+ ion was observed at $h\nu_2 \sim 26\,080\,cm^{-1}$ and the appearance of the CO^+ ion was 30 cm^{-1} lower than the ionization threshold. An estimated shift of the ionization potential by using Eq. (14) is $\Delta = -33$ cm^{-1}, which agrees well with the appearance energy of CO^+ ion in Fig. 13(b). In addition, the intensity drop of the C(^3P) yield spectrum and the appearance of the CO^+ ion occur at the same ν_2 frequency. Thus, it is concluded that the intensity drop of the C(^3P) yield spectrum in the energy region below IP_0 is due to the field ionization.

IV. CONCLUSION

In this work, we observed the Rydberg series converging to the $CO^+(X\,^2\Sigma^+)$ ion in the region of 88–97 nm by C and O fragment atoms yield spectra and the ion-dip spectra. The observed spectra were also compared with the simulated spectra based on the l-uncoupling model. Anomalous inten-

sities are observed for several states, representing the parity and J-dependent predissociation. It was found that np and nf states for $n=4-6$ show the strong parity dependence of their dissociation rate constants. Especially, $L\,^1\Pi(v'=0)$ and $L'\,^1\Pi(v'=1)$ are strongly coupled to the spin-forbidden channel leading to $C(^1D)+O(^3P)$. At high np series, the parity and J-dependence of predissociation become weaker and the simulated spectra without any selectivity of the dissociation agree with the observed spectra. In the spectra of the nf series, the Q branch intensities are comparable to the P, R branches in the $C(^3P)$ yield spectra, which are different from the ion-dip spectra. It is concluded that the nf states predissociate through not only the $D'\,^1\Sigma^+$ valence state but also the $2\,^1\Pi$ state, and the the predissociation rate of the f-symmetry component is slower than that of the e-symmetry component. At higher n-Rydberg states, it is suggested that the np Rydberg states ($n=9-18$) are strongly perturbed by other states because of the complexity of the $C(^3P)$ yield spectrum. For the future work, the detection of the other fragment atoms, that is, $C(^1D)$, $O(^3P)$, and $O(^1D)$, would be important in the investigation of the mechanism and dynamics of the predissociative Rydberg states of CO.

[1] M. Ogawa and S. Ogawa, J. Mol. Spectrosc. **41**, 393 (1972).
[2] S. Ogawa and M. Ogawa, J. Mol. Spectrosc. **49**, 454 (1974).
[3] C. Letzelter, M. Eidelsberg, F. Rostas, J. Breton, and B. Thieblemont, Chem. Phys. **114**, 273 (1987).
[4] M. Eidelsberg and F. Rostas, Astron. Astrophys. **235**, 472 (1990).
[5] M. Eidelsberg, J. J. Benayoun, Y. Viala, and F. Rostas, Astron. Astrophys., Suppl. Ser. **90**, 231 (1991).
[6] P. F. Levelt, W. Ubachs, and W. Hogervorst, J. Chem. Phys. **97**, 7160 (1992).
[7] K. S. E. Eikema, W. Hogervorst, and W. Ubachs, Chem. Phys. **181**, 217 (1994).
[8] W. Ubachs, K. S. E. Eikema, P. F. Levelt, W. Hogervorst, M. Drabbels, W. L. Meerts, and J. J. ter Meulen, Astrophys. J. Lett. **427**, L55 (1994).
[9] W. Ubachs, K. S. E. Eikema, W. Hogervorst, and P. C. Cacciani, J. Opt. Soc. Am. B **14**, 2469 (1997).
[10] M. Drabbels, J. Heinze, J. J. ter Meulen, and W. L. Meerts, J. Chem. Phys. **99**, 5701 (1993).
[11] S. R. Mackenzie, E. J. Halse, E. Gordon, D. Rolland, and T. P. Softley, Chem. Phys. **209**, 127 (1996).
[12] N. Hosoi, T. Ebata, and M. Ito, J. Phys. Chem. **95**, 4182 (1991).
[13] T. Ebata, N. Hosoi, and M. Ito, J. Chem. Phys. **97**, 3920 (1992).
[14] M. Komatsu, T. Ebata, and N. Mikami, J. Chem. Phys. **99**, 9350 (1993).
[15] M. Komatsu, T. Ebata, T. Maeyama, and N. Mikami, J. Chem. Phys. **103**, 2420 (1995).
[16] G. L. Wolk and J. W. Rich, J. Chem. Phys. **79**, 12 (1983).
[17] D. L. Cooper and K. Kirby, J. Chem. Phys. **87**, 424 (1987).
[18] W. ÜL. Tchang-Brillet, P. S. Julienne, J. M. Robbe, C. Letzelter, and F. Rostas, J. Chem. Phys. **96**, 6735 (1992).
[19] J. Baker, W. ÜL. Tchang-Brillet, and P. S. Julienne, J. Chem. Phys. **102**, 3956 (1995).
[20] M. Hiyama and H. Nakamura, Chem. Phys. Lett. **248**, 316 (1996).
[21] M. Hiyama, N. Kosugi, and H. Nakamura, J. Chem. Phys. **107**, 9370 (1997).
[22] J. Tennyson, J. Phys. B **29**, 6185 (1996).
[23] B. E. Forch and C. N. Merrow, J. Chem. Phys. **95**, 3252 (1991).
[24] C. N. Merrow and B. E. Forch, J. Chem. Phys. **93**, 4791 (1990).
[25] W. T. Hill III, B. P. Turner, H. Lefebvre-Brion, S. Yang, and J. Zhu, J. Chem. Phys. **92**, 4272 (1990).
[26] A. Okazaki, T. Ebata, T. Sutani, and N. Mikami, J. Chem. Phys. **108**, 1765 (1998).
[27] S. N. Dobryakov and Y. S. Levedev, Sov. Phys. Dokl. **13**, 873 (1969).
[28] S. V. O'Neil and H. F. Schaefer III, J. Chem. Phys. **53**, 3994 (1970).
[29] T. Ebata, Y. Anezaki, M. Fujii, N. Mikami, and M. Ito, J. Phys. Chem. **87**, 4773 (1983).
[30] S. Rośen, R. Peverall, M. Larsson, A. Le Padellec, J. Semaniak, Å. Larson, C. Strömholm, W. J. van der Zande, H. Danared, and G. H. Dunn, Phys. Rev. A **57**, 4462 (1998).
[31] W. A. Chupka, J. Chem. Phys. **98**, 4520 (1993).
[32] S. T. Pratt, J. Chem. Phys. **98**, 9241 (1993).